

Development and Stability Analysis of LSD-Based Virtual Synchronous Generator for HVDC Systems

A. Musa, *Member, IEEE*, A. Kaushal, S.K. Gurumurthy, D. Raisz, *Member, IEEE*,
F. Ponci, *Senior Member, IEEE*, A. Monti, *Senior Member, IEEE*

Abstract—This paper proposes the Linear Swing Dynamics-based Virtual Synchronous Generator (LSD-VSG) for HVDC systems. The aim is to define a new role and behavior for HVDC systems in their participation to AC system frequency support. This results in enhancing the frequency stability of HVDC connected-AC grids based on the LSD concept, whereas preserving a stable operation of HVDC system. Small signal stability and parametric sensitivity analysis have been performed to support the viability of the proposed LSD-VSG and study the sensitivity of the critical eigenvalues to the closed loop system states and corresponding stability region. Additionally, various time-domain simulations are performed and the results prove the effectiveness and features of the LSD-VSG.

Index Terms—HVDC system, Linear Swing Dynamics, stability analysis, Virtual Synchronous Generator.

I. INTRODUCTION

The High Voltage DC (HVDC) transmission technology is currently deemed a desirable option for long distance power transmission and offshore wind power delivery [1], [2]. According to the recommendations and grid connection requirements set by the European Network of Transmission System Operators for Electricity [3], the HVDC systems are expected to participate in system frequency support. However, the incessant integration of offshore and onshore Renewable Energy Sources (RESs) will displace the existing Synchronous Generators (SGs) resulting in a reduced system inertia. Consequently, the system frequency stability and dynamic performance are affected. Note that classical SGs offer significant advantages such as inherent inertial response, system synchronization, and primary power reserve. However, the main downside of these SGs is the nonlinear characteristics, i.e. nonlinear swing dynamics, which is caused by the inherent nonlinear electromechanical oscillations. This is in contrast with the RESs, which are integrated to the power grid via static converters, as these converters do not have the problem of inherent electromechanical oscillations. Hence, in future converter-based power systems, new concepts should be developed to define system dynamics and behavior. In this regard, the Linear Swing Dynamics (LSD) concept is proposed in [4] and [5] to achieve uniform and linear system swing dynamics. Also, to exploit the fast dynamics, smartness, and controllability of these converters to shape freely system

dynamic behavior. It is worth mentioning that future converter-based power systems will feature fast dynamics, with impact on control and automation. In such a scenario, HVDC systems are expected to take on new roles and behaviors in supporting and strengthening of AC power systems.

There are several works investigating system frequency support through HVDC systems. In [6] and [7], the authors proposed Synchronverter for grid-tied HVDC converter to emulate the classical SG thus providing virtual inertia and system frequency support. However, their proposed Synchronverter is implemented based on the classical representation of SG represented by the nonlinear swing dynamics. In this work, a new design of VSG is proposed for HVDC systems, based on the LSD concept. This aim is to define the role and behavior of HVDC systems in participating of frequency support for future converter-based systems. In [8], the authors presented a model of grid-tied Virtual Synchronous Generator (VSG) based on classical representation of SG. Then, small signal model is derived to assess the stability by analyzing the eigenvalues and their parametric sensitivities. This work derives a mathematical model of the proposed LSD-VSG in two-terminal HVDC system. Then, a linearized small-signal model is obtained to perform eigenvalue based stability analysis and parametric sensitivities. In [4] and [5], the authors proposed the LSD-VSG for grid-tied RES converters, i.e. for onshore RES application. The aim is to define a linear dynamical behavior to the VSG while providing virtual inertia and frequency support. This paper presents the extension of the work in [4] and [5] by designing LSD-VSG for grid-tied HVDC converters, i.e. for offshore RES application. The rationale behind introducing LSD in HVDC systems is that in future power systems, the converter-based power generation will be likely from onshore RES and HVDC (offshore RES or international power exchange) systems [5]. Hence, it is important to introduce and embed the LSD concept in all these grid-tied converters to achieve LSD characteristics in a systematic way. Also, to define the behavior of HVDC systems with regard to system frequency support. Small signal stability and parametric sensitivity analyses has been performed to support the viability of the proposed LSD-VSG. Also, to study the impact of controller states on the dominant eigenvalues and corresponding stability regions. Hence, to provide a holistic design insight for control parameters for which the system is stable, meaning that the analysis allows a numerical parametrization in design of current and voltage controller.

The authors are with the Institute for Automation of Complex Power Systems, RWTH Aachen University, 52074 Aachen, Germany.

*Corresponding author (AMusa@eonerc.rwth-aachen.de)

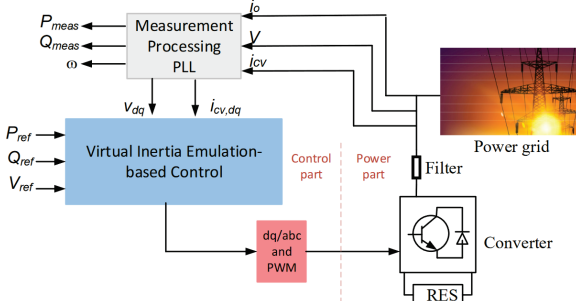


Fig. 1. Virtual Synchronous Generator

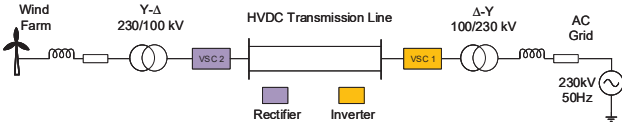


Fig. 2. Two-terminal HVDC System

Additionally, time-domain simulations have been conducted under different scenarios. The results show the effectiveness and performance of the LSD-VSG in achieving the LSD characteristics in the HVDC-connected AC grid, preserving stable DC voltage profile, and providing system frequency support.

II. SYSTEM DESCRIPTION

Two terminal HVDC system is considered to deliver the power from offshore wind farm to the onshore AC grid as shown in Fig. 2. The length, rated power and nominal voltage for HVDC transmission line has been considered as 70 km, 200 MVA and +/-100 kV, the voltage and frequency for onshore AC grid are 230 kV and 50 Hz respectively as per [9]. As the focus of this work is to support and strengthen the AC grid, the LSD-VSG is implemented in the grid-tied HVDC converter (VSC1). The converter VSC1 regulates the DC link voltage based on active power-voltage droop mode, controls AC voltage and provides frequency support based on the LSD concept. On the other hand, the wind farm-tied converter (VSC2) operates in a constant power mode to deliver the rated wind power to the onshore AC grid.

III. PROPOSED LSD-BASED VSG CONTROL

This section presents the controls for LSD and VSG in detail together with their proposed structure in the two-terminal system. Firstly, the VSG is implemented in the grid-tied HVDC converter to synchronize the latter with the AC grid, and hence, making it responsive and supportive in case of disturbances in the AC grid. Secondly, the LSD concept is introduced to achieve the LSD characteristics while providing system frequency support.

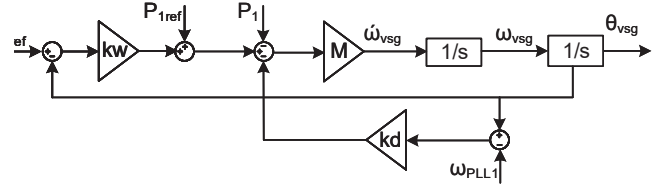


Fig. 3. VSG Control loop

A. Virtual Synchronous Generator

One well-known solution for inertia control is the VSG, with the converter emulating the classical SG and participating in virtual inertia provision. The VSG consists of two stages: the power part and control part as illustrated in Fig. 1 [5]. The VSG is implemented based on the so called swing equation. More details about VSG can be found in [10] and [11]. In this work, the VSG implementation is carried out as presented in [8] and shown in Fig. 3. The converter control has been implemented in a synchronously rotating reference frame (SRF) using dq axis decoupling. The frequency (ω_{vsg}) and phase angle reference (θ_{vsg}) for the control system are provided by the VSG control loop, by incorporating the inertia emulation loop according to the following equation:

$$\dot{\omega}_{vsg} = M(P_{1ref} - P_1) - Mkd(\omega_{ref} - \omega_{PLL1}) - kw(\omega_{ref} - \omega_{vsg}) \quad (1)$$

where the values of kd and M in above equation are $1*10^8$ and $0.14*10^{-3}$, respectively.

B. Linear Swing Dynamics (LSD) Concept

The LSD concept is proposed in [5] and [4] to achieve a uniform and linear swing dynamics for future converter-based power systems. Hence, to have linear and well-predictable system dynamics. This in turn, aims to preserve system stability under small and large disturbances. This can be achieved with the exploitation of smartness, controllability, and fast dynamics of the deployed grid-tied converters. Thanks to the power electronics for their substantial role in shaping freely future system dynamics and behavior. To derive the mathematical formulation for LSD concept, the considered AC system is represented by a Single Machine Infinite Bus (SMIB) system as depicted in Fig. 4. The power angle characteristics of a SMIB system is expressed by (2), which is used to analyze system transient stability

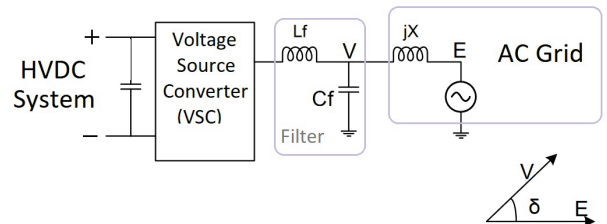


Fig. 4. Symbolic power system

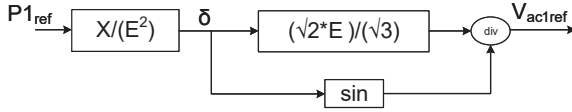


Fig. 5. Control diagram for LSD

$$P = \frac{EV}{X} \sin \delta \quad (2)$$

where \$P\$, \$E\$, \$V\$, \$X\$, and \$\delta\$ are the active power generated by the converter, bus terminal AC voltage, converter terminal voltage, grid impedance (\$X \gg R\$), and the angle between \$E\$ and \$V\$. The equation (2) shows a non-linear relationship between \$P\$ and \$\delta\$ which in turn depicts the non-linear behavior of the system. This non-linearity imposes critical restrictions and limitation on the control converter's design and performance. In this regard, the LSD concept has been introduced to linearize (2) by introducing the AC voltage tolerance \$\epsilon\$, the equation can be re-written as:

$$P = \frac{E}{X}(1 - \epsilon)E\delta \quad (3)$$

where \$\epsilon\$ is the AC voltage tolerance which is set to +/- 0.1 and +/- 0.05 percent of the nominal voltage in distribution and transmission systems respectively. From (2) and (3), the following can be obtained:

$$\delta(P) = \frac{PX}{(1 - \epsilon)E^2} \quad (4)$$

$$V(\delta) = \frac{(1 - \epsilon)E}{\sin \delta} \quad (5)$$

\$V(\delta)\$ in equation above yields the AC voltage reference at every power generation/loading level of the converter so that the power-angle (\$P\$-\$\delta\$) characteristic is linear and can be implemented in the control logic as illustrated in Fig. 5. The AC voltage reference is fed to the outer AC voltage control of the grid tied HVDC converter (VSC1). More information about LSD concept features and application can be found in [5] and [4].

C. Control Structure of LSD-VSG

Fig. 6 shows the control structure of the LSD-VSG in the grid-tied converter that controls the DC link voltage based on active power-voltage droop, and achieves the LSD characteristics while maintaining the AC voltage around the nominal value, and providing frequency support in case of disturbances in the AC grid. On the other hand, the wind farm-tied converter has the role of controlling the active and reactive power generated by the wind farm in accordance to the load in AC grid, as shown in Fig. 7. The aim is to maximize the active power delivered via HVDC system to the AC grid and minimize the reactive power. The control parameters are provided in Table II in the Appendix. Note that the role of

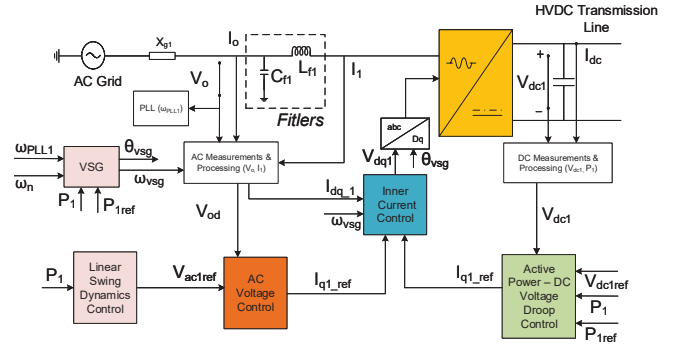


Fig. 6. Proposed LSD-VSG for grid-tied HVDC converter

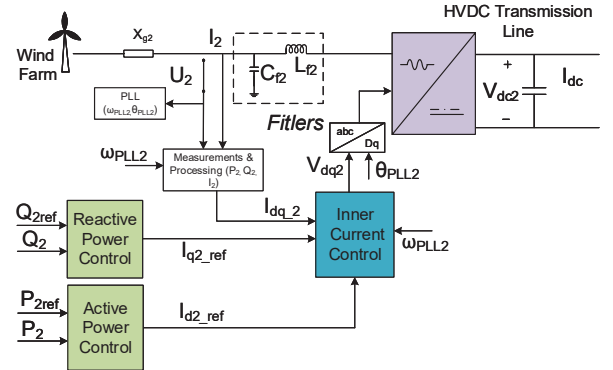


Fig. 7. Control diagram for wind farm-tied converter (VSC2)

LSD concept is to achieve linear \$P\$ - \$\delta\$ characteristics, capture the complete information of and preserve system stability in case of small and large disturbances. These features are more significant for grid side than offshore RES. However, the LSD concept can also be introduced and achieved in the RES-tied converter.

The presented LSD concept relies on the AC voltage tolerance to achieve linear \$P\$ - \$\delta\$ characteristics. However, this can be achieved by different approaches, i.e., without using the AC voltage control and its tolerance. This is currently being developed by the authors.

IV. STATE-SPACE MODELLING & SMALL-SIGNAL STABILITY ANALYSIS (SSSA)

The closed loop mathematical modeling of the two terminal HVDC system under consideration is developed as provided in the Appendix. The resulting state space equations are non-linear equations containing physical state variables with additional mathematical state variables that are augmented for describing the existing PI current and voltage controllers. For performing eigenvalue based stability analysis, the non-linear state-space model is linearized around a steady-state operating point. The objective of the stability analysis is to

obtain the bounds of the control parameters for which the LSD control stabilizes the two terminal network. Thus, the stability analysis offers design insight on choosing control parameters. Furthermore, a sensitivity analysis is performed to investigate the influence of LSD control on dominant eigenvalues. Results obtained from the above sensitivity analysis shows the most critical control parameters that should be considered for the design process. A stability heat-map is presented to illustrate the stable and unstable regions for variation in the control parameter. Thus the boundaries of the stability region show the upper and lower bounds of control parameters.

The state vector X and input vector U can be defined as follows: $X = [I_{d1} \ x_{d1} \ y_{d1} \ I_{q1} \ x_{q1} \ y_{q1} \ V_{dc1} \ I_{dc} \ V_{dc2} \ I_{d2} \ x_{d2} \ y_{d2} \ I_{q2} \ x_{q2} \ y_{q2} \ \omega_{vsg} \ V_{od} \ V_{oq} \ I_{od} \ I_{oq}]^T$ and $U = [P_{1ref} \ V_{dc1ref} \ \omega_{ref} \ Q_{2ref}]^T$

This linear time invariant (LTI) closed loop state-space model is given by (6)

$$\Delta \dot{X} = A \Delta X + B \Delta U \quad (6)$$

where A and B matrices in above equation are the linearized state transition and control matrix respectively. The stability can be determined via the eigenvalues of matrix A . The eigenvalue plot showing the stable operation of the HVDC interconnection is shown in Fig. 8 where the zoomed portion shows the most critical eigenvalues that are highly influenced by the choice of control parameters. In Fig. 8, the most critical eigenvalues EV1, EV2 and EV3 are encircled in green and the less critical eigenvalues EV4, EV5 and EV6 are encircled in pink.

VSC1 which consists of the proposed LSD-VSG control technique is the object of investigation and the control parameters involved in VSC1 will be altered to study closed loop stability. The control parameters in VSC2 remain unaltered for the investigation to clearly illustrate the features of LSD-VSG.

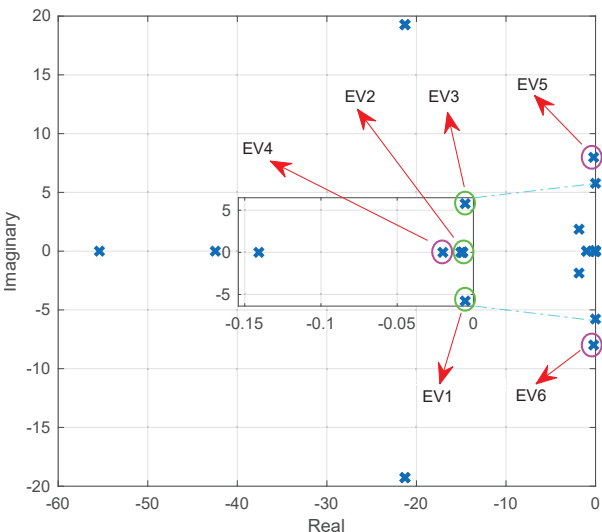


Fig. 8. Eigenvalues for the System

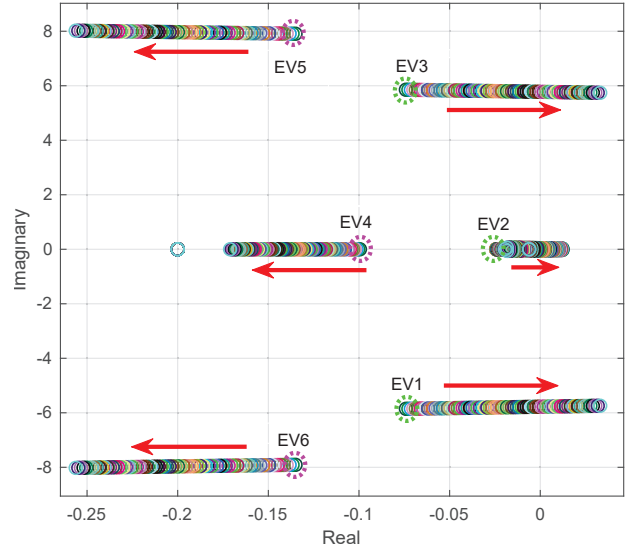


Fig. 9. Variation of eigenvalues with variation of current controller parameter

Fig. 9 shows the root locus plot of critical eigenvalues when the proportional gain of the inner current controller (k_{pd1}) varies from 0.2 to 1.2. With a fixed k_{id1} , it is observed that the system becomes unstable for $k_{pd1} > 0.75$. The critical eigenvalues EV1, EV2 and EV3 move to the right half plane (RHP) making the system unstable. An identical analysis is performed with the integral gain of the voltage controller (k_{ivdc1}) where the gain is varies from 20 to 60. As shown in Fig. 10 , the three dominant poles EV1, EV2 and EV3 move to the RHP for values greater than 45 making the system unstable. VSC1 is implemented with the LSD loop where the swing dynamics are linear, hence small signal stability analysis needs to be applied for various power references. Fig. 11 shows the root locus of active power variation. Note that the active power set-points are varied from -2 p.u to 2 p.u to study a wide operating range for LSD-VSG, in both rectification and inversion mode. However, for the presented two terminal HVDC system, the stability analysis is valid for power variation from 0 to 2 p.u.

From the above analysis, the impact of control parameters and active power set-points on system stability were identified. The unstable operation occurs for active power set-points lesser than -1.5 p.u. With more negative values of active power reference, the eigenvalues tend to have small real part and large imaginary part which leads to increased power oscillations in the system. EV1 and EV3 are complex conjugate poles and their imaginary part becomes larger for negative active power set-points. On the other hand, EV2 is a real pole and it moves to the RHP for active power set-points lesser than -1.5 p.u contributing to system instability. Referring to Fig. 11, it is worth mentioning that the system is stable for power variation from 0 to 2 p.u.

To further examine the system, a relative parametric sensitivity analysis is conducted to investigate the influence of

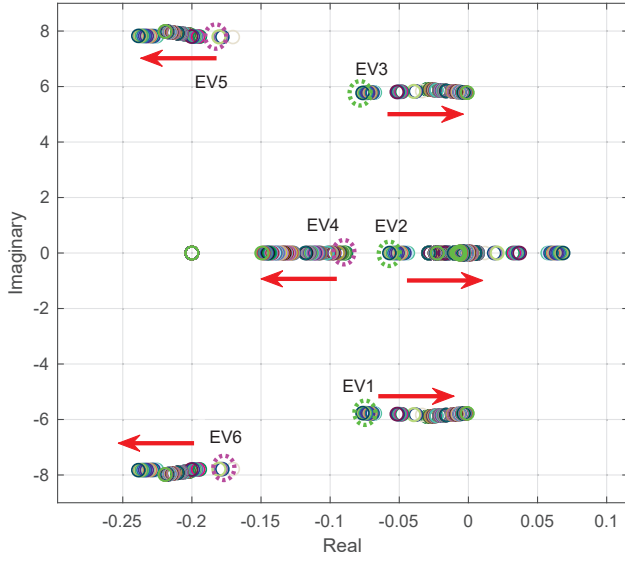


Fig. 10. Variation of eigenvalues with variation of voltage controller parameter

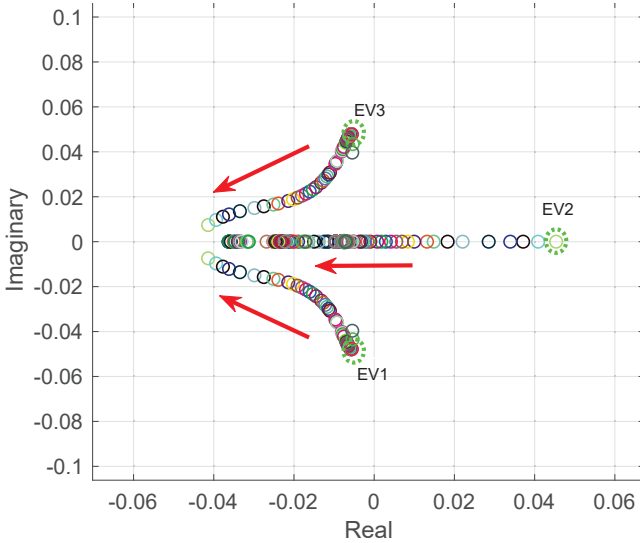


Fig. 11. Variation of eigenvalues with variation of reference power value

the states on the dominant eigenvalues EV1 and EV2 in accordance to the method described in [11]. Fig.12 shows the relative sensitivity analysis for EV1, where the relative sensitivity of critical eigenvalues to state variable variation is plotted. One can observe that the internal states corresponding to the dq voltage controller (x_{d1} and x_{q1}) highly influence the dominant pole EV1. Similarly, as observed from Fig. 14, the internal states of the dq current controller (y_{d1} and y_{q1}) highly influence EV2. Thus, the previous analysis provides the rational to further investigate the stability and instability regions of the current and voltage controller wherein one obtains a design insight.

Fig. 13 and Fig.15 display the heat-map of the variation of

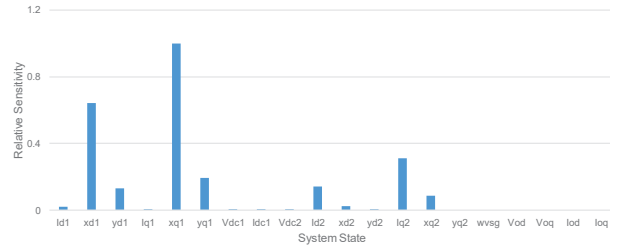


Fig. 12. Relative Parametric Sensitivity of System states for EV1

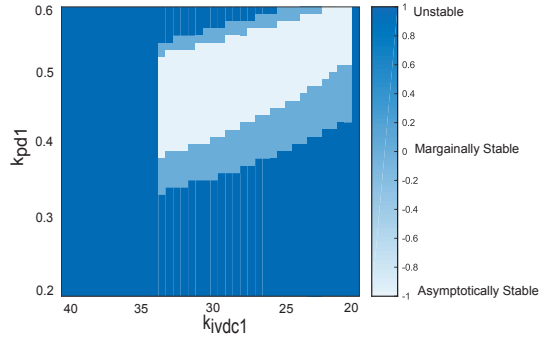


Fig. 13. Heat-map for variation of EV1 for control parameters

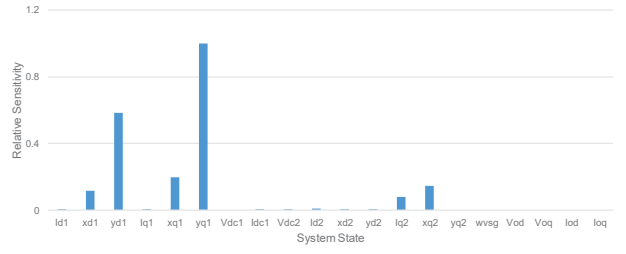


Fig. 14. Relative parametric sensitivity of system states for EV2

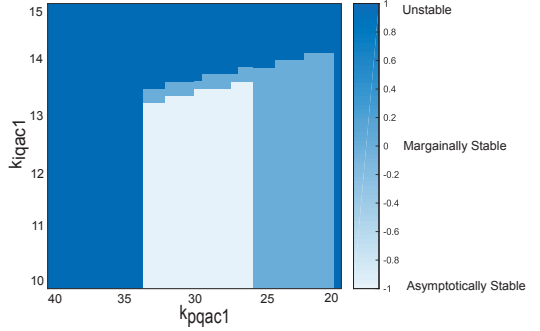


Fig. 15. Heat-map for variation of EV2 for control parameters

the dominant eigenvalues EV1 and EV2 with respect to variation in the voltage and current control parameters obtained from the parametric sensitivity analysis respectively. Dark blue color in these figures represents an unstable system whereas light blue and white color represents marginally stable and asymptotically stable system respectively. The small-signal

stability analysis is repeated for various control parameter combination to obtain the heat-map.

For the inner current control, the lower and upper boundaries of the proportional and integral gains are obtained as shown in Fig. 15, for which the system is stable. Note that any combination of k_{pqac1} and k_{iqac1} , from the white region, yields a stable current control design. Similarly, the lower and upper boundaries of k_{pd1} and k_{ivdc1} are determined for the outer voltage control as depicted in Fig. 13.

It is worth mentioning that the performed small-signal stability analysis in this paper can be used as a tool for control design parameterization wherein the designer is supported with a visual aid such as heat-map for choosing the control gains.

The control parameters are defined in a unified manner for all circumstances. From the stability analysis, we select the most stabilizing solutions which would work for both small and large disturbances. The selected parameters are therefore verified by performing large signal time domain simulations.

V. SIMULATION RESULTS

To scrutinize the performance of the proposed LSD-VSG control scheme, the presented HVDC system has been tested and simulated in MATLAB Simulink. Fig. 16 illustrates the loading in time for AC grid1. This is done by increasing the power demand from 0.3 to 0.6 p.u. in the time instant 4 s, and up by 0.3 p.u. at the following time instants 6 and 8 s, to reach 1.2 p.u. The objective of these test scenarios is to verify the LSD-VSG feature of preserving a stable HVDC system operation, enabling the grid-tied HVDC converter (LSD-VSG) to operate with a linear dynamic behavior to provide virtual inertia and frequency support. Note that the focus of this paper is on the validation of LSD concept, and hence, only the simulation results for grid-tied converter VSC1, i.e. LSD-VSG, are presented.

The increase in power demand is supplied by the power injected from LSD-VSG (P) as depicted in Fig. 17. This in turn, caused an increase in the angle (δ) as shown in Fig. 21. According to the LSD concept presented in Subsection III.B, the LSD loop updates the AC voltage reference, which is fed to the AC voltage control, in a way to achieve the LSD characteristics. Hence, for the applied test scenarios, the AC voltage is regulated within the permitted tolerance as depicted in Fig. 19, and the linear relationship has been achieved between P and δ as shown in Fig. 22.

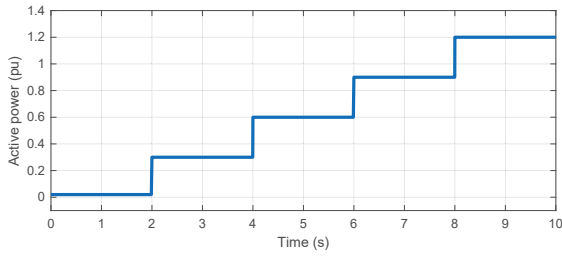


Fig. 16. Change in load active power

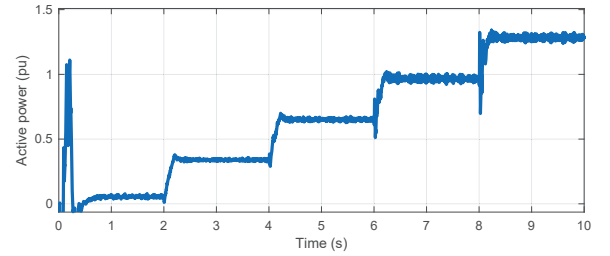


Fig. 17. Active power injected by HVDC link

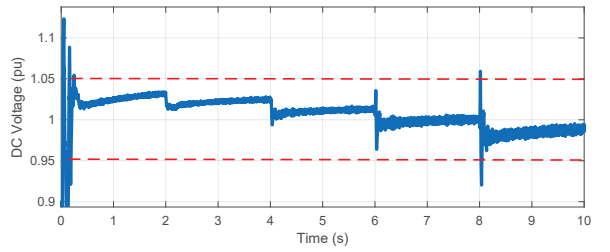


Fig. 18. DC link voltage

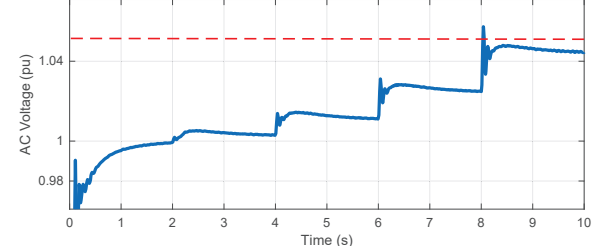


Fig. 19. AC system voltage

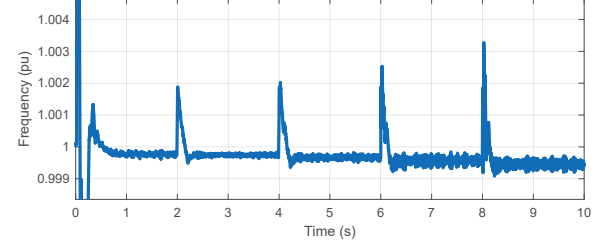


Fig. 20. Frequency of VSG

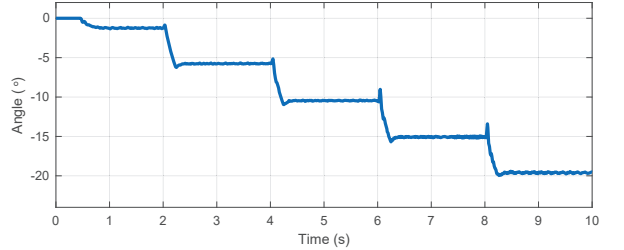


Fig. 21. Angle (δ) variation

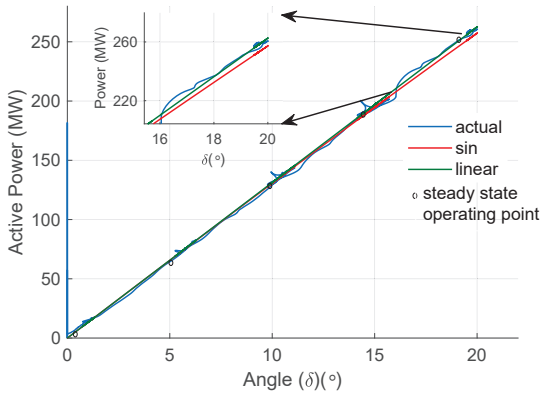


Fig. 22. Power-angle characteristics for the system

The magnification in Fig. 22 aims to clearly show the actual system response with the intermediate transients. It is to be noted that the red colored (sinusoidal) line represents the nonlinear P- δ characteristics of a SG as well as other proposed solutions, which are developed based on classical emulation of SG, i.e., by adopting the nonlinear P- δ characteristics. However, a comparative study between the proposed LSD-VSG and other classical solutions is being conducted by the authors, to be published in future work.

From the conducted scenarios, it can be observed that the LSD-VSG is able to provide frequency support to the AC grid while maintaining a stable DC voltage profile as shown in Fig. 20 and Fig. 18, respectively. Note that the dash lines (in red color) shown in Fig. 18 and Fig. 19 represent the steady state tolerance for DC and AC voltages, respectively.

It is to be noted that with the introduction of LSD, the grid-tied HVDC converter behaves like a Synchronous generator exhibiting Linear Swing (P- δ) characteristics. This linear Synchronous Generator can preserve a stable operation even with countering a large disturbance as shown and verified in the presented large signal simulations.

VI. CONCLUSION

In this work, the LSD-VSG for HVDC systems delivering the wind power to an AC grid has been developed, tested and validated. Stability analysis has been performed to support the viability of the LSD-VSG and provide a holistic design approach for the control parametrization. Also, time domain simulations are conducted and the results show that the proposed LSD-VSG is able to achieve the LSD characteristics while providing frequency support and preserving stable HVDC system operation. The LSD characteristics and features are attained by achieving linear P- δ characteristics and preserving stable system operation, in both small disturbance (as observed in the stability analysis) and large disturbances (as shown in the time domain simulations).

The influence of varying the droop and inertial terms, in LSD-VSG control, on LSD characteristics and overall system dynamic performance will be studied in future work.

ACKNOWLEDGMENT

This article is part of RESERVE project that has received funding from the European Union's Horizon 2020 research and innovation programme under grant agreement N 727481. Also, the authors gratefully acknowledge funding by the German Federal Ministry of Education and Research (BMBF) within the Kopernikus Project ENSURE New ENergy grid StructURes for the German Energiewende.

REFERENCES

- [1] A. S. Elansari, S. J. Finney, J. Burr and M. F. Edrah, Frequency control capability of VSC-HVDC transmission system, 11th IET International Conference on AC and DC Power Transmission, 2015.
- [2] D. Van Herterm, O. Gomis-Bellmunt, and J. Liang, HVDC Grids For Offshore and Supergrid of the Future, John Wiley & Sons, New Jersey, 2016.
- [3] Commission Regulation (EU) 2016/1447, Establishing a Network Code on Requirements of High Voltage Direct Current Systems and Direct Current Connected Power Park Modules, 2016.
- [4] A. Musa, A. Monti, et.al. Linear Swing Dynamics (LSD) Concept Validation and Application in Future Converter-Based Power Systems, EU-H2020 RESERVE Project, Deliverable D2.3, March 2018.
- [5] D. Raisz, A. Musa, F. Ponci, A. Monti, Linear and Uniform System Dynamics of Future Converter-Based Power Systems, IEEE PES General Meeting, Portland, USA, 2018.
- [6] R. Aouini, B. Marinescu, et.al., Synchronvreter-Based Emulation and Control of HVDC Transmission, IEEE Transaction on Power Systems, vol. 31, pp. 278-286. 2016.
- [7] E. Rajan, Amrutha S, Synchronverters: Synchronverter Based HVDC Transmission, IEEE International Conference on Innovations in Power and Advanced Computing Technologies, pp. 1-6, 2017.
- [8] S. D'Arco, J. Are Suul, O. B. Fosso, A Virtual Synchronous Machine implementation for distributed control of power converters in Smart Grids, Journal of Electric Power Systems Research, vol. 122, pp. 180-197, 2015.
- [9] H. Ouquelle, L. A. Dessaint, and S. Casoria, An average value model-based design of a deadbeat controller for VSC-HVDC transmission link, IEEE Power Energy Society General Meeting, pp. 1-6, 2009.
- [10] T. Shintai, Y. Miura and T. Ise, Oscillation Damping of a Distributed Generator Using a Virtual Synchronous Generator, IEEE Transactions on Power Delivery, Vol. 29, No. 2, pp. 668 - 676, 2014.
- [11] S. D'Arco, J. A. Suul and O. B. Fosso, Control system tuning and stability analysis of Virtual Synchronous Machines, IEEE Energy Conversion Congress and Exposition, pp. 2664-2671, 2013.

VII. APPENDIX

State-space equations

$$\begin{aligned} \frac{dI_{d1}}{dt} = & \frac{1}{L_f} (-k_{pd1}k_{pvdc1}\beta P_{1ref} + k_{pd1}k_{pvdc1}\beta P_1 \\ & - k_{pd1}k_{pvdc1}(V_{dc1ref} - V_{dc1}) - k_{pd1}k_{ivdc1}x_{d1} \\ & + k_{pd1}I_{d1} - k_{id1}y_{d1}) \end{aligned} \quad (7)$$

$$\frac{dx_{d1}}{dt} = \beta(P_{1ref} - P_1) + (V_{dc1ref} - V_{dc1}) \quad (8)$$

$$\begin{aligned} \frac{dy_{d1}}{dt} = & -I_{d1} - k_{pvdc1}\beta P_1 - k_{pvdc1}V_{dc1} + k_{ivdc1}x_{dc1} \\ & + k_{pvdc1}\beta P_{1ref} + k_{pvdc1}V_{dc1ref} \end{aligned} \quad (9)$$

$$\begin{aligned} \frac{dI_{q1}}{dt} = & \frac{1}{L_f} (-k_{pq1}k_{pqac1}V_{ac1ref} - k_{pq1}k_{pqac1}V_{od} \\ & + k_{pq1}k_{iqac1}x_{q1} + k_{pq1}I_{q1} - k_{iq1}y_{q1}) \end{aligned} \quad (10)$$

$$\frac{dx_{q1}}{dt} = (V_{ac1ref} - V_{od}) \quad (11)$$

$$\frac{dy_{q1}}{dt} = -I_{q1} + k_{pqac1}V_{ac1ref} - k_{pqac1}V_{od} + k_{iqac1}x_{q1} \quad (12)$$

$$\frac{dV_{dc1}}{dt} = \frac{P_1 + rI_{d1}^2 + rI_{q1}^2}{V_{dc1}C_{eq}} + \frac{I_{dc}}{C_{eq}} \quad (13)$$

$$\frac{dI_{dc}}{dt} = \frac{V_{dc2}}{L_{dc}} - \frac{r_{dc}I_{dc}}{L_{dc}} - \frac{V_{dc1}}{L_{dc}} \quad (14)$$

$$\frac{dV_{dc2}}{dt} = \frac{U_{d2}I_{d2} - rI_{d1}^2 - rI_{q1}^2}{V_{dc2}C_{eq}} - \frac{I_{dc}}{C_{eq}} \quad (15)$$

$$\begin{aligned} \frac{dI_{d2}}{dt} = & -\frac{r}{L_f}I_{d2} - \frac{k_{pd2}I_{d2}}{L_f} + \frac{k_{pd2}P_{2ref}}{U_{ac}L_f} \\ & + \frac{k_{pd2}k_{ip21}x_{d2}}{L_f} + \frac{k_{ip22}y_{d2}}{L_f} \end{aligned} \quad (16)$$

$$\frac{dx_{d2}}{dt} = \frac{P_{2ref}}{U_{ac}} - \frac{U_{d2}I_{d2}}{U_{ac}} \quad (17)$$

$$\frac{dy_{d2}}{dt} = \frac{p_{2ref}}{U_{ac}} + k_{ip21}x_{d2} - I_{d2} \quad (18)$$

$$\begin{aligned} \frac{dI_{q2}}{dt} = & -\frac{r}{L_f}I_{q2} - \frac{k_{pq2}I_{q2}}{L_f} - \frac{k_{pq2}Q_{2ref}}{U_{ac}L_f} \\ & + \frac{k_{pq2}k_{iq21}x_{q2}}{L_f} + \frac{k_{iq22}y_{q2}}{L_f} \end{aligned} \quad (19)$$

$$\frac{dx_{q2}}{dt} = -\frac{Q_{2ref}}{U_{ac}} - \frac{U_{d2}I_{q2}}{U_{ac}} \quad (20)$$

$$\frac{dy_{q2}}{dt} = -\frac{Q_{2ref}}{U_{ac}} + k_{iq21}x_{q2} - I_{q2} \quad (21)$$

$$\begin{aligned} \omega_{vsg} = & M(P_{1ref} - P_1) - Mkd(\omega_{ref} - \omega_{PLL1}) \\ & - kw(\omega_{ref} - \omega_{vsg}) \end{aligned} \quad (22)$$

$$\frac{dI_{od}}{dt} = \frac{1}{L_g}V_{od} - \frac{r_g}{L_g}I_{od} + \omega_{vsg}I_{oq} \quad (23)$$

$$\frac{dI_{oq}}{dt} = \frac{1}{L_g}V_{oq} - \frac{r_g}{L_g}I_{oq} + \omega_{vsg}I_{od} \quad (24)$$

$$\frac{dV_{od}}{dt} = \frac{1}{C_f}I_{d1} - \frac{1}{C_f}I_{od} + \omega_{vsg}V_{oq} \quad (25)$$

$$\frac{dV_{oq}}{dt} = \frac{1}{C_f}I_{q1} - \frac{1}{C_f}I_{oq} - \omega_{vsg}V_{od} \quad (26)$$

The state variables mentioned above are described in Table I, also the control parameters used in state equations are mentioned in Table II. The filter inductance and capacitance

L_f and C_f are 0.147 H and 2.5 μ F respectively. The grid has resistance $r_g = 1*10^{-5}\Omega$ and inductance $L_g = 0.0827\text{H}$.

For the HVDC transmission line inductance and resistance, L_{dc} and r_{dc} are set to $1.59*10^{-4}$ H/km and $1.39*10^{-3}\Omega/\text{km}$ respectively. The reference value for active power and voltage for HVDC transmission line is set as 1 pu whereas the same for reactive power at the wind farm side is set to 0 pu.

TABLE I
SYSTEM STATES

State	Description
Grid-tied converter	
I_{d1}, I_{q1}	dq-axis current in the converter and filter inductor
x_{d1}, x_{q1}	integrator state for DC voltage control loop
y_{d1}, y_{q1}	integrator state for dq-axis for inner current control loop
V_{od}, V_{oq}	dq-axis voltage at PCC
I_{od}, I_{oq}	dq-axis current at PCC
ω_{vsg}	VSG angular frequency
Windfarm-tied converter	
I_{d2}, I_{q2}	dq-axis current in the converter and filter inductor
x_{d2}, x_{q2}	integrator state for dq-axis for voltage control loop
y_{d2}, y_{q2}	integrator state for dq-axis for current control loop
HVDC Transmission line	
V_{dc1}, V_{dc2}	DC Voltage at terminal-1 & terminal-2
I_{dc}	current in HVDC transmission line

TABLE II
CONTROL PARAMETERS

Parameter	Value
Grid-tied converter	
Voltage controller Proportional gain (k_{pvdc1}, k_{pqac1})	30
Voltage controller Integral gain (k_{ivdc1}, k_{iqac1})	15
Current controller Proportional gain (k_{pd1}, k_{pq1})	0.42
Current controller Integral gain for d axis (k_{id1}, k_{iq1})	3.2
Windfarm-tied converter	
Voltage controller Proportional gain for d axis (k_{ip21}, k_{iq21})	10
Voltage controller Integral gain for d axis (k_{ip21}, k_{iq21})	50
Current controller Proportional gain for d axis (k_{pd2}, k_{pq2})	0.6
Current controller Integral gain for d axis (k_{ip22}, k_{iq22})	6